Silver(I) Chalcogenide Halides $Ag_{19}Te_6Br_7$, $Ag_{19}Te_6Br_{5.4}I_{1.6}$, and $Ag_{19}Te_5SeBr_7$

Tom Nilges,* Julia Messel, Melanie Bawohl, and Stefan Lange

Institut für Anorganische und Analytische Chemie, Universität Münster, Corrensstrasse 30, 48149 Münster, Germany

Received February 12, 2008. Revised Manuscript Received March 18, 2008

Systematic examinations for new phases on the quasi-binary section $AgX-Ag_2Q$ (with X = halide and Q = chalcogenide) led to the exploration of the three new compounds $Ag_{19}Te_6Br_7$, $Ag_{19}Te_6Br_{5.4}I_{1.6}$, and $Ag_{19}Te_5SeBr_7$. All of them crystallize in new structure types with rigid anion and highly disordered silver substructures. A peritectic decomposition to the binary halides and chalcogenides and $Ag_{23}Te_{12}Br$ was observed for each compound between 693 and 719 K. Polymorphism, a common feature for solid state ion conductors, was found for $Ag_{19}Te_6Br_7$. Impedance spectroscopic investigations showed high conductivities (up to $\sigma = 1.1 \times 10^{-2}\ \Omega^{-1}\ cm^{-1}$, 323 K, $Ag_{19}Te_6Br_{5.4}I_{1.6}$) and low activation energies ($E_a = 0.19$ eV, α-$Ag_{19}Te_6Br_7$) at room temperature. A topological description of the rigid and complex anion substructure was used to classify the three different structures. Linearly arranged nets of anions, separated from each other by the disordered silver ions, corrugate under partial substitution of either the halide or chalcogenide ions. The topological approach is a fundamental tool to understand the structure property relations in more detail.

1. Introduction

Mixed conductors are potential candidates to play a significant role in the development and the improvement of nano-scaled integrated circuits.[1–3] The chalcogenides for instance are favorable mixed conducting materials to build up nano-scaled switches due to their whisker forming properties.[4] Also some coinage metal halides, mainly based on AgI and CuI, the so called ASICs (advanced superionic conductors), gained reasonable interest as new materials for micro(nano)electronics and microsystem technology (MST).[5] The combination of ion mobility and electric conductivity is important to generate fast and reversible electronic contacts between the electrodes.

Recently we started a systematic examination of the ternary system coinage metal−chalcogen−halogen in order to develop new mixed conducting materials. We succeeded in the exploration of a new class of compounds, the silver(I) polychalcogenide halides.[6–10] Those compounds enter the phase field among AgX (with X = halide), Ag_2Q (with Q = chalcogenide), and chalcogen and are characterized by isolated and covalently bonded chalcogen substructures. Nevertheless we also tried to explore the quasi-binary section between AgX and Ag_2Q in more detail. Starting from the purely ion conducting silver halides, the electric properties switch towards a mixed conduction on heading towards Ag_2Q [for a complete overview see ref 6]. Several compounds exist on the quasi-binary section $AgX-Ag_2Q$, featuring the compositions Ag_3QX,[11–13] Ag_5Q_2X,[14–17] and Ag_6TeBr_4,[18] which show different grades of substitution within the anion substructures.[19–24] Karbanov et al. and Blachnik et al. have reported phase analytical results of the quasi-binary section $AgX-Ag_2Te$.[14,18,25] Karbanov et al. postulated a eutectic system with two distinct compounds Ag_3TeBr and Ag_6TeBr_4. Later on Blachnik and coworkers could not reproduce Ag_6TeBr_4, but they found some evidence for the existence of Ag_3TeBr. Unfortunately, a closer characterization of Ag_3TeBr was not performed, and only a hexagonal unit cell was postulated. Interestingly, the electrical properties of

* Corresponding author. Fax: +49-251-83-36636. Phone: +49-251-83-36645. E-mail: nilges@uni-muenster.de.

(1) Waser, R.; Aono, M. *Nat. Mater.* **2007**, *6*, 833.
(2) Terabe, K.; Hasegawa, T.; Nakayama, T.; Aono, M. *Nature* **2005**, *433*, 47.
(3) Maier, J. *Nat. Mater.* **2005**, *4*, 805.
(4) van Ruitenbeek, J. *Nature* **2005**, *433*, 21.
(5) Andreeva, A. V.; Despotuli, A. L. *Ionics* **2005**, *11*, 152.
(6) Lange, S.; Nilges, T. *Chem. Mater.* **2006**, *18*, 2538.
(7) Lange, S.; Bawohl, M.; Wilmer, D.; Meyer, H.-W.; Wiemhöfer, H.-D.; Nilges, T. *Chem. Mater.* **2007**, *19*, 1401.
(8) Nilges, T.; Bawohl, M.; Lange, S. *Z. Naturforsch.* **2007**, *62b*, 955.
(9) Nilges, T.; Bawohl, M. *Z. Naturforsch* **2008**, *63b*, in press.
(10) Lange, S.; Bawohl, M.; Nilges, T. *Inorg. Chem.* **2008**, *47*, 2625.
(11) Reuter, B.; Hardel, K. *Naturwissenschaften* **1961**, *48*, 161.
(12) Reuter, B.; Hardel, K. *Z. Anorg. Allg. Chem.* **1965**, *340*, 168.
(13) Hull, S.; Keen, D. A.; Gardner, N. J. G.; Hayes, W. *J. Phys.: Condens. Matter* **2001**, *13*, 2295.
(14) Blachnik, R.; Dreisbach, H. A. *J. Solid State Chem.* **1985**, *60*, 115.
(15) Nilges, T.; Nilges, S.; Pfitzner, A.; Doert, T.; Böttcher, P. *Chem. Mater* **2004**, *16*, 806.
(16) Doert, T.; Rönsch, E.; Schnieders, F.; Böttcher, P.; Sieler, J. *Z. Anorg. Allg. Chem.* **2000**, *626*, 89.
(17) Brinkmann, C.; Faske, S.; Vogel, M.; Nilges, T.; Heuer, A.; Eckert, H. *Phys. Chem. Chem. Phys.* **2006**, *8*, 369.
(18) Karbanov, S.; Bontschewa-Mladenowa, Z.; Aramov, N. *Monatsh. Chem.* **1972**, *103*, 1496.
(19) Beeken, R. B.; Menningen, K. L. *J. Appl. Phys.* **1989**, *66*, 5340.
(20) Beeken, R. B.; Wright, T. J.; Sakuma, T. *J. Appl. Phys.* **1999**, *85*, 7635.
(21) Nilges, T.; Dreher, C.; Hezinger, A. *Solid State Sci.* **2005**, *7*, 79.
(22) Nilges, T.; Lange, S. *Z. Anorg. Allg. Chem.* **2004**, *630*, 1749.
(23) Nilges, T.; Lange, S. *Z. Kristallogr.* **2005**, (Suppl. 22), 173.
(24) Nilges, T.; Lange, S. *Z. Anorg. Allg. Chem.* **2005**, *631*, 3002.
(25) Blachnik, R.; Kundermann, K. *Z. Naturforsch.* **1973**, *28b*, 1.

10.1021/cm800425u CCC: $40.75
Published on Web 05/27/2008

Table 1. Preparation Details and Maximal Grades of Substitution of the Silver(I) Chalcogenide Halides

compound	annealing time (days)	temperature (K)	max. grade of substitution
$Ag_{19}Te_6Br_7$	14	663	
$Ag_{19}Te_6Br_{7-x}Cl_x$	16	618	$x = 1.25$
$Ag_{19}Te_6Br_{7-y}I_y$	21	633−653	$y = 1.75$
$Ag_{19}Te_{6-a}S_aBr_7$	15	633	$a = 0.4$
$Ag_{19}Te_{6-b}Se_bBr_7$	14	643	$b = 1.1$
$Ag_{19-z}Cu_zTe_6Br_7$	14	663	$z = 2.0$

Ag_3TeBr were reported by Beeken et al. without any deeper characterization of the examined compound.[26]

Herein we report on the preparation and characterization of $Ag_{19}Te_6Br_7$, $Ag_{19}Te_6Br_{5.4}I_{1.6}$, and $Ag_{19}Te_5SeBr_6$ representing three new compounds on the quasi-binary section $AgX-Ag_2Q$. Thermal and phase analytical measurements, structural investigations, and an electrochemical characterization were performed in order to shed some light onto the controversial discussion of the Ag_3TeBr problem. A topological approach, first being introduced to assist the structure description and to understand the structure chemistry of $Ag_{10}Te_4Br_3$[7] and $Ag_{23}Te_{12}X$ (with X = Cl, Br),[10] will be used to describe the complex structural features of the title compounds.

2. Experimental Section

2.1. Synthesis. $Ag_{19}Te_6Br_7$ and the solid solutions $Ag_{19}Te_6Br_{7-x}Cl_x$, $Ag_{19}Te_6Br_{7-y}I_y$, $Ag_{19}Te_{6-a}S_aBr_7$, $Ag_{19}Te_{6-b}Se_bBr_7$, and $Ag_{19-z}Cu_zTe_6Br_7$ were prepared from stoichiometric mixtures of Ag (Chempur, 99.9%), Cu (Chempur, 99.999%), S (Chempur, 99.999%), Se (Chempur, 99.999%), Te (Chempur, 99.999%), AgCl (AlfaAesar, 99.9%), AgBr (Chempur, >99%), and AgI (Sigma Aldrich, 99%). All starting materials were used without further purification. The mixtures were sealed in evacuated silica ampoules, heated to 1200 K, held at this temperature for 1 day, and quenched in an ice bath. After homogenization by grinding the samples were annealed at temperatures between 618 and 663 K for 2−3 weeks. The annealing temperature for $Ag_{19}Te_6Br_{7-y}I_y$ was decreased linearly with the increase of the iodide content. Preparation details and maximal grades of substitution are summarized in Table 1.

2.2. Powder Diffraction. To verify the phase purity of the compounds X-ray powder diffraction experiments (2θ range: 5−60°) were performed using a STOE StadiP diffractometer, equipped with a linear 5° position sensitive detector (PSD, Braun). Finely ground samples were examined in transmission geometry applying Cu Kα_1 radiation ($\lambda = 1.54051$ Å, germanium monochromator).

2.3. Single Crystal Diffraction. The intensity data of single crystals were collected on a STOE IPDS II at room temperature using monochromated Mo Kα radiation ($\lambda = 0.71073$ Å, graphite monochromator). After the correction of the data sets for Lorentz, polarization, and absorption effects, the structures were solved by direct methods applying the Shelxs program.[27] Absorption corrections based on optimized crystal shapes from symmetry equivalent reflections were performed prior to all structure refinements using the programs X-Shape and X-Red.[28] All space groups were derived from a careful analysis of the extinction rules. Structure refinements were done with the program package JANA2000.[29]

Table 2. Results from EDX Analyses of Different Silver(I) Chalcogenide Halides

compound	composition (theoretical in atom %) Ag:[Te, Se]:[Br, I]	composition (EDX in atom %) Ag:[Te, Se]:[Br, I]
$Ag_{19}Te_6Br_7$	59.4:18.8:21.9	57(2):20(2):23(2)
$Ag_{19}Te_6Br_{5.4}I_{1.6}$	59.4:18.8:[16.9, 5.0]	54(2):18(2):[22(2), 6(2)]
$Ag_{19}Te_5SeBr_7$	59.4:[15.6, 3.1]:21.9	57(2):[16(2), 5(2)]:22(2)

The high silver mobility and the pronounced silver disorder of all compounds were described using a nonharmonic approach using a Gram−Charlier expansion[30,31] of the Debeye−Waller factor in the refinements. A minimum number of silver positions were introduced to the structure models to minimize the number of split positions and correlations. The procedure of non-harmonic refinement[32−35] is well suited for all ion conducting materials as it has been shown for many other materials in this field.[36−39,7,15,21] The significance of the 3rd order terms was checked by an analysis of the joint probability density functions (jpdf) showing negative regions of not more than 5% of the positive pdf values. Maxima of the probability density, the so-called mode positions (suffix *m* in the atom names in Table 4), were calculated for $Ag_{19}Te_6Br_7$. These mode positions are given in Table 4, in addition to the conventional harmonic coordinates. All distances to the anions, as stated in the supplement, are related to the mode positions in the case of $Ag_{19}Te_6Br_7$. The extraction of the mode positions after jpdf analysis for $Ag_{19}Te_6Br_{5.4}I_{1.6}$ and for $Ag_{19}Te_5SeBr_7$ did not significantly improve the structure models. The conventional positions were used instead.

At this point we have to emphasize that the silver distribution we derived from the single crystal data, for the highly disordered cation substructure, is only an averaged picture and that the reported positions of the silver atoms, within all structures, cannot be used for a detailed bond distance discussion. The X-ray structure determination can only deliver an averaged structure model, and real-structure methods like HR-TEM should be used instead. Unfortunately, the present compounds are not stable under HR-TEM conditions refusing such real-structure analyses.

2.4. Phase Analyses (EDX). Semiquantitative analysis was performed with a Leica 420i scanning electron microscope (Zeiss) fitted with an electron dispersive detector unit (Oxford). Ag, HgTe (Te), KBr (Br), KCl (Cl), FeS_2 (S), Se, and Cu were used as standards for calibration. A voltage of 20 kV was applied to the samples. Details concerning the compositions of all compounds are summarized in Table 2.

2.5. Thermal Analyses. DSC measurements were performed on a NETZSCH differential scanning calorimeter DSC 204 under N_2 atmosphere. Finely ground samples were measured in the temperature range of 113−473 K (in Al crucibles) and of 293−873

(26) Beeken, R. B.; Wang, S. M.; Smith, D. R. *Solid State Ionics* **1992**, *53−56*, 220.
(27) Sheldrick, G. M. *Shelxs-97, Program of Crystal Structure Refinement*; University of Göttingen: Göttingen, Germany, 1997.
(28) *X-Shape*, Ver. 2.05; *X-Red*, Ver. 1.10 (program packages); Stoe & Cie GmbH: Darmstadt, 2005.
(29) Petricek, V.; Dusek, M.; Palatinus, L. *Jana 2000 - The crystallographic computing system*; Institute of Physics: Prague, Czech Republic, 2000.
(30) Johnson, C. K.; Levy, H. A. *International Tables for X-ray Crystallography*; Kynoch Press: Birmingham, 1974; Vol. IV, pp 311−336.
(31) Kuhs,W. F.; Heger, G. *Fast Ion Transport in Solids*; Elsevier: Amsterdam, 1979; pp 233−236.
(32) Kuhs, W. F. *Acta Crystallogr., Sect. A* **1992**, *48*, 80.
(33) Willis, B. M. T. *Acta Crystallogr., Sect. A* **1969**, *25*, 277.
(34) Bachmann, R.; Schulz, H. *Acta Crystallogr., Sect. A* **1984**, *40*, 668.
(35) Zucker, U. H.; Schulz, H. *Acta Crystallogr., Sect. A* **1982**, *38*, 563.
(36) Zucker, U. H.; Schulz, H. *Acta Crystallogr., Sect. A* **1982**, *38*, 568.
(37) Boucher, F.; Evain, M.; Brec, R. *J. Solid State Chem.* **1993**, *107*, 332.
(38) Evain, M.; Bindi, L.; Menchetti, S. *Acta Crystallogr., Sect. B* **2006**, *62*, 768.
(39) Evain, M.; Bindi, L.; Menchetti, S. *Acta Crystallogr., Sect. B* **2006**, *62*, 447.

Table 3. Selected Crystallographic Data of $Ag_{19}Te_6Br_7$, $Ag_{19}Te_6Br_{5.4}I_{1.6}$, and $Ag_{19}Te_5SeBr_7$ at 298 K[a]

empirical formula	$Ag_{19}Te_6Br_7$	$Ag_{19}Te_6Br_7$	$Ag_{19}Te_6Br_{5.4}I_{1.6}$	$Ag_{19}Te_5SeBr_7$
formula weight (g mol^{-1})	3374.5	3374.5	3449.7	3325.8
crystal system	trigonal	monoclinic	orthorhombic	orthorhombic
space group	$R\bar{3}m$	$C2/m$	$Pnma$	$Pbam$
lattice parameters				
a (Å)	7.855(1)	13.604(2)	15.442(3)	15.298(2)
b (Å)		7.857(2)	7.889(2)	38.847(4)
c (Å)	44.184(7)	15.395(2)	26.089(4)	7.830(1)
β (deg)		107.13(1)		
V (Å^3)	2360.8(5)	1572.5(5)	3178.2(11)	4653.2(10)
Z	3	2	4	6
ρ_{calcd} (g cm^{-1})	7.12	7.12	7.25	7.12
crystal size (μm^3)	40 × 25 × 20	40 × 25 × 20	60 × 40 × 40	40 × 30 × 20
absorption coeff. (mm^{-1})	25.9	25.9	25.2	26.5
F(000)	4350	2900	5913	8604
θ-range (deg)	2−26	2−26	2−28	1−26
hkl-range	−9/9, −9/+9, −55/+54	±15, 0/+9, 0/+19	−19/20, −10/10, −33/34	±18, −42/47, ±9
reflections collected	4146	4171	21551	29848
independent reflns. (R_{int})	668 (0.0748)	1517 (0.0496)	2877 (0.1366)	4748 (0.1988)
reflections $I > 3\sigma(I)$	380	572	855	653
reflections/parameters	668/115	1517/250	2877/475	4748/784
goodness of fit (F^2)	1.82	1.15	0.84	0.47
R-values ($I > 3\sigma(I)$) $R1$	0.0728	0.043	0.0417	0.0225
$wR2$	0.0980	0.0492	0.0498	0.0221
R-values (all) $R1$	0.1182	0.1254	0.1596	0.2475
$wR2$	0.1018	0.0607	0.0667	0.0507
$\rho_{max/min}$, e Å^{-3}	2.52/−1.45	1.34/−1.31	1.42/−1.60	1.08/−1.07

[a] The supplementary material has been sent to the Fachinformationzentrum Karlsruhe, Abt. PROKA, 76344 Eggenstein-Leopoldshafen, Germany, as supplementary material CSD 419161 ($Ag_{19}Te_6Br_7$, $R\bar{3}m$), 419160 ($Ag_{19}Te_6Br_7$, $C2/m$), 419159 ($Ag_{19}Te_6Br_{5.4}I_{1.6}$), and 419158 ($Ag_{19}Te_5SeBr_7$), and can be obtained by contacting the FIZ (quoting the article details and the corresponding CSD number).

K (in evacuated silica tubes), respectively, with heating and cooling rates of 10 K/min. Hg, In, Bi, Zn, and CsCl were used for temperature calibration. For the thermal analysis above 473 K the samples were sealed in evacuated silica ampoules.

2.6. Impedance Spectroscopy. Total conductivities of the samples were measured with a Novocontrol standard sample cell BDS 1200 using a Novocontrol alpha-S impedance analyser. A frequency range of 10 mHz and 3 MHz was applied in a temperature range of 173 and 323 K. Ion blocking gold electrodes were sputtered to cold pressed pellets, and impedance spectra were recorded under an oxygen and moisture free nitrogen atmosphere. An equilibration time of 1−5 min was used between each measurement in order to achieve temperature constancy.

3. Results and Discussion

Recently we started a systematic investigation to stabilize new silver chalcogenide halides on the quasibinary section $AgX-Ag_2Q$ (X = halide; Q = chalcogenide). All efforts to prepare a compound with the postulated nominal composition Ag_3TeBr via common solid state melting reactions or mineralization routes using Te(IV) halides failed. Instead we could stabilize a chalcogenide halide with a closely related composition of $Ag_{3.167}TeBr_{1.167}$ ($Ag_{19}Te_6Br_7$). EDX analyses of selected crystals substantiated the composition as summarized in Table 2.

A preparation of the compound with the derived composition directly led to phase pure products.

Thermal and electric properties were determined by DSC and impedance spectroscopic experiments. The new silver chalcogenide halide is a mixed conductor with an enhanced total conductivity. Solid solutions with a permutation of the anions and the exchange of silver by copper were prepared in order to tune the physical properties of the new compound. We could successfully prepare the solid solutions $Ag_{19}Te_{6-a}S_aBr_6$, $Ag_{19}Te_{6-b}Se_bBr_6$, $Ag_{19}Te_6Br_{7-x}Cl_x$, $Ag_{19}Te_6Br_{7-y}I_y$, and $Ag_{19-z}Cu_zTe_6Br_7$ with various substitution grades.[40] The two new quaternary compounds are representatives of the highly substituted ends of the solutions while the $Ag_{19}Te_6Br_7$ type is realized for low substitution grades. Further details of the solid solutions will be reported elsewhere, and quantitative analyses of the measured single crystals are given in Table 2.

All title compounds show peritectic decomposition at temperatures slightly above 673 K. Details concerning the different experiments and the properties will be given in the following sections.

3.1. Crystal Structures. Silver chalcogenides and halides are representatives of a class of materials with highly disordered cation substructures. This feature is caused by an enhanced silver mobility leading to polymorphism and high ion conductivity. A preservation of these properties can be observed for the binary as well as for the ternary phases.

Intensity data for the three different silver(I) chalcogenide halides were collected on an IPDS II diffractometer. Tables 3–6 summarize the crystallographic data of all single crystal structure determinations. Two different structure models are considered for $Ag_{19}Te_6Br_7$. A brief discussion of this aspect is given in the following section.

We have developed a topological approach to describe the complex structures by simple structural units like strands and nets. Those strands and nets are defined by anion−anion distances within or slightly above the range of the sum of the van der Waals radii of the respective ions. We will show at the end of this section that the subdivision into different anion units can help to understand the structure chemistry of the silver(I) chalcogenide halides in more detail. What we cannot do is to directly transfer some developed concepts

(40) Nilges, T.;Messell, J. Z. *Anorg. Allg. Chem.* **2008**, *634*, in press.

Table 4. Atomic Positions and Isotropic Displacement Parameters (Å^{-2}) of $Ag_{19}Te_6Br_7$ at 298 K

atom	Wyckoff	sof	x	y	z	U_{eq}
			$Ag_{19}Te_6Br_7$ ($R\bar{3}m$)			
Te1	6*c*	1	0	0	0.0509(4)	0.0598(11)
Te2	6*c*	1	0	0	0.16015(8)	0.0767(14)
Te3	6*c*	1	1/3	2/3	0.00058(7)	0.0560(11)
Br1	18*h*	1	0.5001(2)	0.0002(4)	0.09059(6)	0.0490(11)
Br2	3*b*	1	1/3	2/3	1/6	0.050(2)
Ag1	36*i*	0.427(9)	0.328(3)	0.305(3)	0.1415(6)	0.292(10)
Ag2	18*h*	0.624(18)	0.777(3)	0.8884(15)	0.1106(4)	0.303(11)
Ag3	36*i*	0.312(18)	−0.007(5)	0.702(4)	0.0215(13)	0.26(2)
Ag4	18*h*	0.17(3)	0.132(3)	0.868(3)	−0.0036(7)	0.23(5)
Ag5	18*h*	0.25(2)	0.1970(16)	0.8030(16)	0.0468(3)	0.112(15)
Ag6	6*c*	0.376(17)	1/3	2/3	0.0553(5)	0.123(9)
Ag7	18*h*	0.40(2)	0.2040(19)	0.408(4)	−0.0424(8)	0.240(17)
Ag8	6*c*	0.34(18)	1/3	2/3	−0.0562(2)	0.080(7)
			mode position			
Ag1m			0.3273	0.3255	0.1425	
Ag2m			0.7646	0.8823	0.1095	
Ag3m			0.0001	0.6806	0.0203	
Ag4m			0.1191	0.8809	−0.0039	
Ag6m			0.3333	0.6667	0.0574	
Ag7m			0.1948	0.3896	−0.0469	
			$Ag_{19}Te_6Br_7$ ($C2/m$)			
Te1	4*i*	1	−0.0509(2)	0	−0.1524(1)	0.0575(7)
Te2	4*i*	1	0.8399(2)	0	0.5193(1)	0.0723(9)
Te3	4*i*	1	0.3340(2)	0	0.0019(1)	0.0552(8)
Br1	4*i*	1	0.5910(2)	0	0.2716(2)	0.0474(9)
Br2	2*d*	1	0	1/2	1/2	0.048(1)
Br3	8*j*	1	0.3399(2)	0.2505(2)	0.27154(12)	0.0473(6)
Ag1	8*j*	0.315(12)	0.465(2)	−0.374(3)	0.435(2)	0.342(16)
Ag2	8*j*	0.427(16)	0.310(2)	−0.1741(14)	0.4551(17)	0.351(16)
Ag3	8*j*	0.396(17)	0.651(2)	0.229(2)	0.4175(12)	0.535(19)
Ag4	8*j*	0.322(17)	0.9398(16)	0.2286(19)	0.6183(14)	0.352(12)
Ag5	8*j*	0.374(16)	0.5497(14)	−0.383(3)	0.3138(10)	0.261(12)
Ag6	8*j*	0.173(13)	0.6358(18)	−0.354(2)	0.3204(9)	0.238(12)
Ag7	4*i*	0.28(2)	0.238(2)	0	0.311(2)	0.38(3)
Ag8	4*i*	0.29(2)	0.285(3)	0	0.369(2)	0.147(17)
Ag9	8*j*	0.388(13)	0.4863(15)	−0.224(2)	−0.0423(12)	0.245(10)
Ag10	8*j*	0.319(13)	0.3307(15)	−0.370(3)	−0.0565(13)	0.205(11)
Ag11	8*j*	0.447(16)	0.3791(14)	−0.363(2)	0.0449(13)	0.302(12)
Ag12	8*j*	0.334(10)	0.0462(9)	0.2911(11)	−0.1333(8)	0.153(6)
Ag13	4*i*	0.289(14)	0.2371(11)	0	0.1378(7)	0.126(9)
Ag14	4*i*	0.369(9)	0.3865(9)	0	0.1665(5)	0.114(5)
Ag15	4*i*	0.346(9)	0.2785(8)	0	−0.1696(7)	0.086(4)
Ag16	4*i*	0.310(13)	0.1517(17)	0	−0.1362(10)	0.128(8)
Ag17	8*j*	0.31(5)	−0.1545(12)	0.2880(12)	−0.1329(7)	0.162(7)
			mode position			
Ag1m			0.4761	−0.3702	0.423	
Ag2m			0.3185	−0.1658	0.4474	
Ag3m			0.6619	0.1844	0.4147	
Ag4m			0.9553	0.2442	0.6264	
Ag5m			0.5503	−0.3449	0.3211	
Ag7m			0.2253	0	0.3246	
Ag9m			0.4795	−0.19	−0.0523	
Ag10m			0.3285	−0.3403	−0.0617	
Ag11m			0.3665	−0.3513	0.0464	
Ag12m			0.0479	0.2897	−0.1422	
Ag14m			0.3863	0	0.171	
Ag15m			0.2786	0	−0.1641	
Ag16m			0.1421	0	−0.1405	
Ag17m			−0.1447	0.2841	−0.1365	

of structure design and prediction onto this case. For instance the principle of structural evolution of megaseries, like in the broad system A/M′/M″/Se with A = K, Rb, Cs, Sr, Ba; M′ = Pb, Sn; and M″ = Sb, Bi as reported by Mrotzek and Kanatzidis[41,42] and by Makovicki[43] for bismuth−lead sulfosalts cannot be transferred to the present case. On the one hand the defined structure units and nets do not result from direct bond interaction and are only of topological nature, and on the other hand, the severe disorder in the silver substructure refuses to divide the silver substructure into distinct parts. A subdivision in layered arrangements including silver positions which are interconnected by bromide ions can be theoretically postulated on the basis of the rigid anion substructure after calculating their charge and charge-balancing it with silver ions. As a result of the quasi-molten silver substructure and the strongly temperature dependent silver distribution relative to the anions, such a differentiation

(41) Mrotzek, A.; Kanatzidis, M. G. *Acc. Chem. Res.* **2003**, *36*, 111.
(42) Kanatzidis, M. G. *Acc. Chem. Res.* **2005**, *38*, 361.
(43) Makovicky, E. *Fortschr. Mineral.* **1981**, *59*, 137.

Table 5. Atomic Positions and Isotropic Displacement Parameters (Å^{-2}) of $Ag_{19}Te_6Br_{5.4}I_{1.6}$ at 298 K

atom	Wyckoff	sof	*x*	*y*	*z*	U_{eq}
Te1	4*c*	1	0.2008(2)	1/4	0.6006(1)	0.0470(9)
Te2	4*c*	1	−0.3681(2)	1/4	0.7041(1)	0.0632(10)
Te3	4*c*	1	0.1084(2)	3/4	0.7106(1)	0.0630(10)
Te4	4*c*	1	0.0194(2)	3/4	0.5399(1)	0.0513(9)
Te5	4*c*	1	0.4922(2)	3/4	0.4529(1)	0.0569(10)
Te6	4*c*	1	−0.0736(2)	1/4	0.6471(1)	0.0547(10)
Br1	8*d*	0.78(2)	−0.1213(2)	−0.0090(3)	0.7955(1)	0.0457(9)
I1	8*d*	0.22	−0.1213	0.0090	0.7955	0.0457(9)
Br2	4*c*	0.72(4)	0.3147(2)	3/4	0.5806(1)	0.0485(14)
I2	4*c*	0.28	0.3147	3/4	0.5806	0.0485(14)
Br3	4*c*	0.81(3)	−0.1803(2)	3/4	0.6727(1)	0.0451(13)
I3	4*c*	0.19	−0.1803	3/4	0.6727	0.0451(13)
Br4	8*d*	0.81(2)	0.24912(17)	−0.0006(3)	0.4549(1)	0.0453(9)
I4	8*d*	0.18	0.24912	−0.0006	0.4549	0.0453(9)
Br5	4*c*	0.72(3)	−0.4359(2)	3/4	0.6254(2)	0.0457(11)
I5	4*c*	0.28	−0.4359	3/4	0.6254	0.0457(11)
Ag1	4*c*	0.351(1)	−0.2041(8)	3/4	0.7193(7)	0.214(8)
Ag2	4*c*	0.238(7)	0.1761(6)	3/4	0.5163(4)	0.088(4)
Ag3	4*c*	0.192(8)	−0.1320(6)	3/4	0.5735(7)	0.078(5)
Ag4	8*d*	0.43(2)	0.1153(14)	−0.0591(16)	0.6204(6)	0.151(9)
Ag5	4*c*	0.265(7)	0.2665(6)	3/4	0.6889(9)	0.137(6)
Ag6	8*d*	0.20(3)	−0.336(3)	−0.077(3)	0.6871(15)	0.32(2)
Ag7	8*d*	0.433(15)	0.0175(12)	0.110(2)	0.7223(8)	0.209(7)
Ag8	8*d*	0.32(2)	0.075(3)	0.112(3)	0.5360(16)	0.316(16)
Ag9	8*d*	0.25(2)	−0.2558(18)	0.041(2)	0.6577(8)	0.266(12)
Ag10	8*d*	0.407(16)	0.1563(15)	−0.021(3)	0.5470(8)	0.225(10)
Ag11	4*c*	0.190(14)	−0.0217(13)	3/4	0.7486(13)	0.206(11)
Ag12	8*d*	0.44(2)	0.0221(16)	−0.039(2)	0.6388(7)	0.211(9)
Ag13	8*d*	0.379(13)	−0.0765(13)	−0.056(3)	0.5956(8)	0.190(8)
Ag14	8*d*	0.40(2)	−0.348(2)	0.135(3)	0.8089(8)	0.325(16)
Ag15	4*c*	0.17(2)	0.007(3)	3/4	0.7886(16)	0.42(3)
Ag16	8*d*	0.506(18)	−0.1185(8)	0.0833(18)	0.9088(9)	0.262(8)
Ag17	8*d*	0.64(2)	0.4013(14)	0.124(4)	0.4817(9)	0.428(14)
Ag18	8*d*	0.319(13)	0.2078(10)	−0.0270(19)	0.6520(6)	0.131(7)
Ag19	8*d*	0.41(2)	0.2671(14)	−0.155(6)	0.3715(11)	0.39(2)
Ag20	8*d*	0.39(2)	−0.040(2)	−0.038(2)	0.9563(8)	0.308(16)
Ag21	8*d*	0.46(2)	−0.004(2)	0.118(2)	0.5610(7)	0.40(3)
Ag22	4*c*	0.100(11)	0.142(3)	1/4	0.496(3)	0.18(3)
Ag23	4*c*	0.244(18)	−0.284(3)	1/4	0.7910(8)	0.30(2)
Ag24	4*c*	0.082(11)	−0.097(3)	1/4	0.5545(13)	0.29(3)
Ag25	8*d*	0.25(2)	−0.1657(16)	0.172(4)	0.9622(11)	0.282(15)
Ag26	8*d*	0.39(3)	−0.3207(12)	−0.051(3)	0.7145(16)	0.252(15)
Ag27	8*d*	0.66(2)	0.0104(15)	0.1014(19)	0.8696(6)	0.402(13)
Ag28	8*d*	0.28(10)	−0.0145(13)	−0.0389(3)	0.6983(7)	0.141

is not possible. There is no chance to count the silver positions either to the one or the other side. Therefore we focus our attention only on the anion substructure first.

Four different types of units forming net-like arrangements and strands are sufficient to describe the complex anion substructure:

The chalcogenide substructure of $Ag_{19}Te_6Br_7$ is build up by a 6^3 Te^{2-} net unit (1) and a corrugated and Br^- centered Te_6 ring unit in chair conformation (2) as denoted in the structure picture (Figure 1). The latter unit can be formally constructed from the end atoms of a Te_4 unit (4) interpenetrating the 6^3 nets (1). Bromide ions are forming a Kagomé-like 3.6.3.6 net (3) separating the chalcogenide substructure. It has to be stated at this point that no direct bonding interaction is present within those units and all postulated nets are only of a topological nature. In the following we will use this topological approach to describe the crystal structures in more detail.

$Ag_{19}Te_6Br_7$. $Ag_{19}Te_6Br_7$ can be described by an $R\bar{3}m$ model with lattice parameters of $a = 7.855(1)$ Å and $c = 44.184(7)$ Å. The anion substructure is build up by planar 6^3 Te^{2-} nets (1), corrugated Te_6 ring nets (2), and Kagomé-like Br^- nets (3). Te_4 units (4) interpenetrate (1) parallel to the stacking direction of the anion nets. Figure 1 shows the arrangement of the anion nets and the whole crystal structure, featuring the distribution of the disordered silver substructure relative to the anion framework. A certain difference of the silver distribution is present dependent on the neighboring anion substructure. Silver is distributed in a S-shaped manner around the Te_6 rings (2). A more diffuse distribution, but also less pronounced silver displacement is present around the 6^3 nets (1) and Te_4 units (4) (see Figure 1). Interestingly, a gap of the silver distribution can be observed in direct proximity to the Br^- nets (4). This feature was also observed in case of $Ag_{10}Te_4Br_3$ where the gap around the Kagomé-like 3.6.3.6 nets can be closed by an increase of the silver mobility with temperature.[6,7]

Distances within the anion nets range from 4.53 Å to 4.54 Å for the 6^3 net (1), 4.56 Å to 4.57 Å for the Te_6 rings (2), and 3.91 to 3.94 Å for the Br−Br distances in the Kagomé net (3). Bond distances are summarized in the supplement.

A common problem in crystallography is the possible symmetry reduction from the space group $R\bar{3}m$ to $C2/m$ and the decision of which model results in a better or the true description of the structure. In most cases the higher symmetry is sufficient to describe all structural features of a

Table 6. Atomic Positions and Isotropic Displacement Parameters ($Å^{-2}$) for $Ag_{19}Te_5SeBr_7$ at 298 K

atom	Wyckoff position	sof	*x*	*y*	*z*	U_{eq}
Te1	4*g*	1	0.1953(3)	0.2196(1)	0	0.0658(13)
Te2	4*h*	1	0.0860(3)	0.3908(1)	1/2	0.0569(13)
Te3	4*g*	0.94(3)	0.0468(3)	0.4448(1)	0	0.0535(15)
Se3	4*g*	0.06	0.0468	0.4448	0	0.0535(
Te4	4*h*	0.84(4)	0.1746(3)	0.2763(1)	1/2	0.0639(16)
Se4	4*h*	0.16	0.1746	0.2763	1/2	0.0639
Te5	4*g*	0.81(4)	0.5742(3)	0.3862(1)	0	0.0659(17)
Se5	4*g*	0.19	0.5742	0.3862	0	0.0659
Te6	4*h*	0.82(4)	0.1380(3)	0.5170(1)	1/2	0.0706(18)
Se6	4*h*	0.18	0.138	0.517	1/2	0.0706
Te7	4*g*	0.65(3)	0.2669(2)	0.3500(1)	0	0.0508(14)
Se7	4*g*	0.35	0.2669	0.35	0	0.0508
Te8	4*g*	0.53(4)	0.4920(3)	0.1818(1)	0	0.0529(17)
Se8	4*g*	0.47	0.492	0.1818	0	0.0529
Te9	4*h*	0.97(4)	0.5611(3)	0.4483(1)	1/2	0.0723(18)
Se9	4*h*	0.03	0.5611	0.4483	1/2	0.0723
Br1	4*h*	1	0.1286(3)	0.1673(1)	1/2	0.0463(16)
Br2	2*a*	1	1/2	1/2	0	0.050(2)
Br3	4*g*	1	0.2480(4)	0.5298(1)	0	0.0505(16)
Br4	8*i*	1	−0.1850(2)	0.3856(1)	0.2511(4)	0.0467(12)
Br5	4*h*	1	−0.1147(3)	0.3015(1)	1/2	0.0460(16)
Br6	8*i*	1	0.3122(2)	0.44595(8)	0.2497(4)	0.0478(12)
Br7	8*i*	1	0.4442(2)	0.2798(1)	0.2384(4)	0.0499(12)
Br8	4*h*	1	0.3800(3)	0.3632(1)	1/2	0.0483(16)
Ag1	4*g*	0.62(2)	0.3656(11)	0.2296(6)	0	0.192(9)
Ag2	4*h*	0.453(16)	0.2432(15)	0.4051(7)	1/2	0.110(6)
Ag3	8*i*	0.532(17)	0.1955(16)	0.3343(5)	0.2941(19)	0.258(11)
Ag4	4*g*	0.48(2)	−0.100(2)	0.4236(10)	0	0.114(10)
Ag5	4*h*	0.521(18)	0.3281(13)	0.2848(7)	1/2	0.171(10)
Ag6	4*h*	0.51(2)	−0.0568(15)	0.3622(8)	1/2	0.179(11)
Ag7	4*g*	0.40(2)	0.2007(15)	0.4602(15)	0	0.135(16)
Ag8	4*h*	0.516(18)	0.0301(17)	0.2471(10)	1/2	0.190(10)
Ag9	8*i*	0.71(2)	−0.2466(15)	0.2852(5)	0.298(2)	0.313(9)
Ag10	8*i*	0.29(3)	0.143(2)	0.3896(8)	0.124(7)	0.190(19)
Ag11	8*i*	0.292(17)	−0.046(2)	0.4878(8)	0.226(2)	0.198(12)
Ag12	8*i*	0.42(3)	0.523(2)	0.3368(8)	0.184(4)	0.48(2)
Ag13	8*i*	0.53(2)	0.130(2)	0.4856(10)	0.218(3)	0.310(15)
Ag14	8*i*	0.44(2)	−0.079(3)	0.4499(10)	0.235(4)	0.242(16)
Ag15	4*h*	0.44(3)	0.2854(14)	0.5764(6)	1/2	0.261(12)
Ag16	8*i*	0.37(2)	0.5509(19)	0.2217(6)	0.260(4)	0.180(10)
Ag17	8*i*	0.48(3)	−0.1928(15)	0.3237(5)	0.192(5)	0.381(18)
Ag18	8*i*	0.392(19)	0.094(2)	0.2739(8)	0.126(5)	0.359(17)
Ag19	8*i*	0.48(2)	0.079(2)	0.3244(10)	0.290(4)	0.298(17)
Ag20	8*i*	0.48(2)	0.369(2)	0.5992(6)	0.683(2)	0.389(18)
Ag21	8*i*	0.49(3)	0.061(4)	0.3753(6)	0.146(3)	0.30(2)
Ag22	8*i*	0.302(18)	−0.0371(11)	0.3526(6)	0.282(3)	0.143(8)
Ag23	4*h*	0.66(5)	−0.054(4)	0.4391(14)	1/2	0.73(5)
Ag24	8*i*	0.75(3)	0.476(3)	0.4101(14)	0.258(5)	0.95(4)
Ag25	4*h*	0.45(3)	0.156(3)	0.4532(7)	1/2	0.229(19)
Ag26	4*g*	1.05(4)	0.4441(12)	0.4236(7)	0	0.487(17)
Ag27	8*i*	0.598(17)	0.2429(13)	0.2906(3)	0.115(3)	0.453(12)
Ag28	8*i*	0.22(2)	0.441(3)	0.4915(4)	0.333(3)	0.17(2)
Ag29	8*i*	0.28(2)	0.053(4)	0.4515(7)	0.365(3)	0.37(3)
Ag30	4*g*	1.05(8)	−0.267(5)	0.3357(13)	0	1.09(6)
Ag31	8*i*	0.42(3)	0.4170(18)	0.3630(8)	0.139(4)	0.333(16)
Ag32	8*i*	0.33(3)	−0.369(4)	0.308(2)	0.206(6)	0.95(6)
Ag33	8*i*	0.43(2)	0.6370(12)	0.4767(4)	0.251(2)	0.279(9)
Ag34	4*h*	0.66(5)	0.388(3)	0.4764(10)	1/2	0.62(4)
Ag35	8*i*	0.30(2)	0.3025(12)	0.5323(9)	0.654(2)	0.334(16)
Ag36	8*i*	0.397(18)	0.2386(18)	0.3906(6)	0.289(3)	0.259(13)
Ag37	4*g*	0.22(3)	0.460(3)	0.3375(6)	0	0.27(3)
Ag38	4*g*	0.23(3)	0.204(3)	0.4137(7)	0	0.136(17)
Ag39	4*g*	0.4(3)	−0.015(5)	0.3823(14)	0	0.28(5)

compound.[44] In the present case the anion substructure is properly described by the higher symmetry. Nevertheless the high silver dynamic and the large disorder within the silver substructure can better be expressed by the lower symmetry, introducing more parameters to the refinement. Selected crystallographic data, atomic coordinates, and displacement parameters are given in Tables 3 and 4. The doubling of parameters after the symmetry reduction to *C*2/*m* has a certain influence on the residual values and the statistical parameters. The most important improvement is the significant reduction of the residual electron density within the disordered silver substructure. As a result of the high silver ion mobility and the characteristic ion conducting property it is highly recommended to choose the best possible

(44) Baur, W. H.; Kassner, D. *Acta Crystallogr., Sect. B* **1992**, *48*, 356.

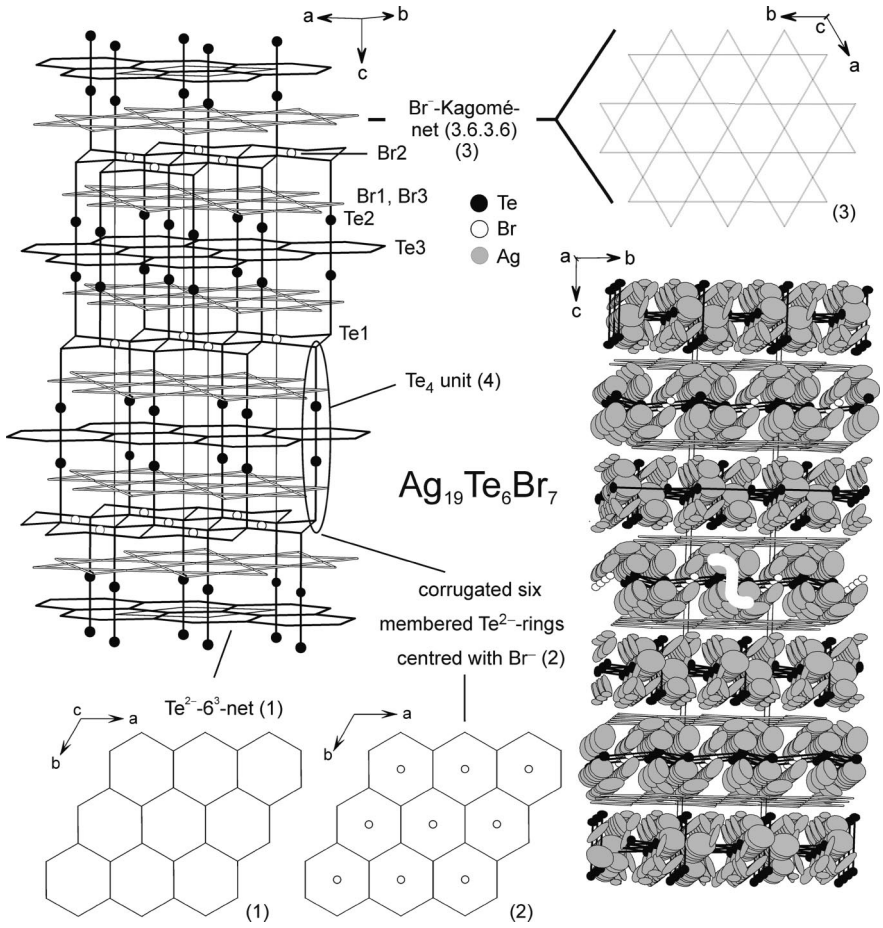

Figure 1. Crystal structure of $Ag_{19}Te_6Br_7$ ($R\bar{3}m$ model). The anion substructure can be described by 6^3 Te^{2-} nets (1), 3.6.3.6 Br^- nets (2), and corrugated, Br^- centered, Te_6 ring nets (3). (1) and (2) are interpenetrated by Te_4 units (4). Silver is completely disordered within the anion substructure. A white symbol denotes the silver distribution around (2). All lines within the nets represent distances close to or slightly above the sum of the respective van der Waals radii. Displacement parameters are at 90 % probability.

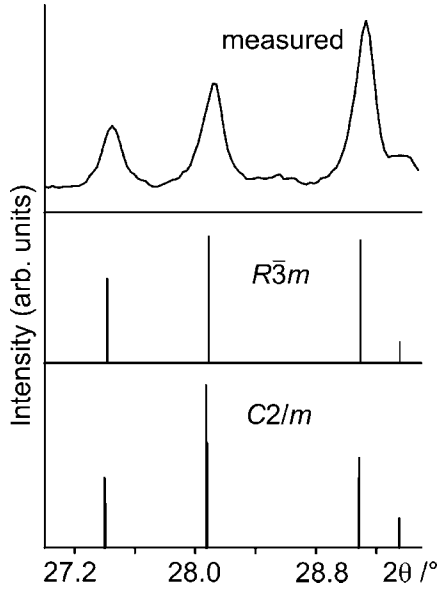

Figure 2. Section of measured and two calculated powder diffractograms of $Ag_{19}Te_6Br_7$ (Cu $K\alpha_1$ radiation). Two structure models, in the space group $R\bar{3}m$ (a = 7.855(1) Å; c = 44.184(7) Å) and the subgroup $C2/m$ (a = 13.604(2) Å; b = 7.857(2) Å; c = 15.395(2) Å; β = 107.13(1)°) are shown. A very small and not resolvable split of reflections can be observed.

description for the whole structure which is $C2/m$ in the present case. To make this fact absolutely clear, from an exclusively crystallographic point of view the structure description in $R\bar{3}m$ is sufficient enough. We have calculated the resulting split of reflections which occurs after the symmetry reduction from $R\bar{3}m$ to $C2/m$ (see Figure 2).

Unfortunately this feature cannot be resolved with common X-ray diffraction experiments, and even a synchrotron experiment may not be able to resolve this split. The present problem demands the determination of the real structure by high resolution transmission electron microscopy (HR-TEM) methods and not the averaged structure as derived from diffraction methods. Unfortunately the silver(I) chalcogenide halides are not stable under HR-TEM conditions refusing such experiments (see also refs 7 and 10). A final decision is maybe possible if the structure of the low temperature phase of $Ag_{19}Te_6Br_7$ (see Section 3.4) is solved and a group−subgroup scheme can be created. A structure determination of the low temperature phase is currently underway.

$Ag_{19}Te_6Br_{5.4}I_{1.6}$. The partial substitution of bromide by iodide results in a completely different arrangement of the formerly introduced units (1)−(4). A statistic distribution of iodide was found over all halide sites without a clear preference of any of the halide positions. In Figure 3 the anion and total structure are illustrated for $Ag_{19}Te_6Br_{5.4}I_{1.6}$. The units (1) and (2) are forming a corrugated net in such a way that two condensed, planar six-membered Te rings of (1), interpenetrated by the Te_4 units (4), are representing a translational subunit of the net. Two corrugated and halide-

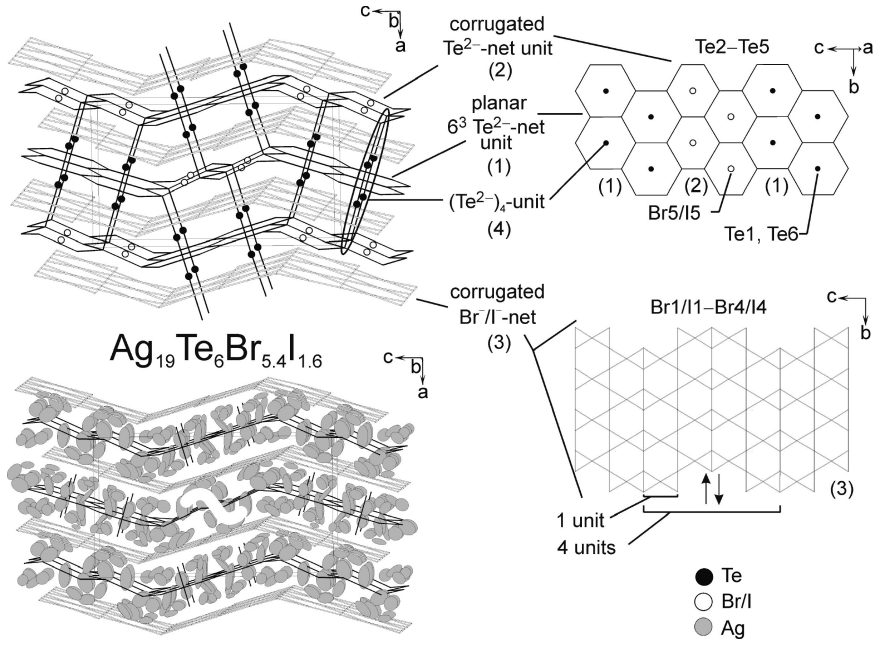

Figure 3. Crystal structure of $Ag_{19}Te_6Br_{5.4}I_{1.6}$. The anion substructure can be described by corrugated nets (1) to (3) and Te_4 units (4). One net is formed by connected, linearly arranged 6^3 Te^{2-} nets (1) and corrugated, Br^-/I^- centered Te_6 ring units (2). The second one, separating the other, is built up by corrugated 3.6.3.6 Br^- nets (3). Silver is completely disordered within the anion substructure. A white symbol denotes the silver distribution around (2). All lines within the nets represent distances close to or slightly above the sum of the respective van der Waals radii. Displacement parameters are at 90 % probability. A bromide subunit and the four linearly connected units forming the Br substructure are illustrated. Arrows show the shearing of those subunits relative to an ideal Kagomé net.

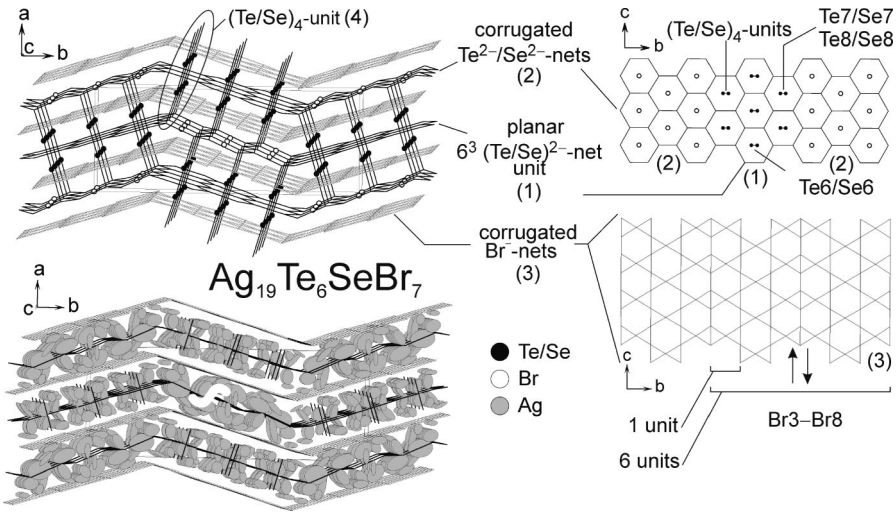

Figure 4. Crystal structure of $Ag_{19}Te_5SeBr_6$. The anion substructure can be described by corrugated nets (1)−(3) and Te_4 units (4). One net is formed by connected, linearly arranged 6^3 (Te/Se) nets (1) and corrugated, Br^- centered $(Te/Se)_6$ ring units (2). The second one, separating the other, is built up by corrugated 3.6.3.6 Br^- nets (3). Silver is completely disordered within the anion substructure. A white symbol denotes the silver distribution around (2). All lines within the nets represent distances close to or slightly above the sum of the respective van der Waals radii. Displacement parameters are at 90 % probability. A bromide subunit and the six linearly connected units forming the Br substructure are illustrated. Arrows show the shearing of those subunits relative to an ideal Kagomé net.

centered Te_6 ring units (2) are attached to the 6^3 units (1) to complete the translation period of the net. The same corrugation can be found for the Kagomé-like halide net with a slightly different arrangement of the halide ions in comparison with the ternary compound. The ideal planar Kagomé-type arrangement (3) of the halide ions in case of $Ag_{19}Te_6Br_7$ is modified for $Ag_{19}Te_6Br_{5.4}I_{1.6}$. A shearing of Kagomé subunits at the contact area of the planar fragments (see Figure 3, right section) occurrs.

Distances within the anion nets range from 4.56 to 4.66 Å for the 6^3 net (1), 4.52 Å to 4.65 Å for the Te_6 rings (2), and 3.80 to 4.08 Å for the Br/I−Br/I distances in the Kagomé net (3). Bond distances are summarized in Supporting Information.

The silver distribution is directly comparable to the ternary compound. In relation to the anion nets and especially to the building units (1)−(4), silver tends to behave in a similar manner. An S-shaped arrangement around (2) and a more localized distribution in the neighborhood of (1) and (4) comes along with a gap of the silver distribution close to the halide nets (4).

$Ag_{19}Te_5SeBr_7$. After the successful modification of the halide substructure a partial substitution of the chalcogenide substructure was performed. The substitution resulted in a

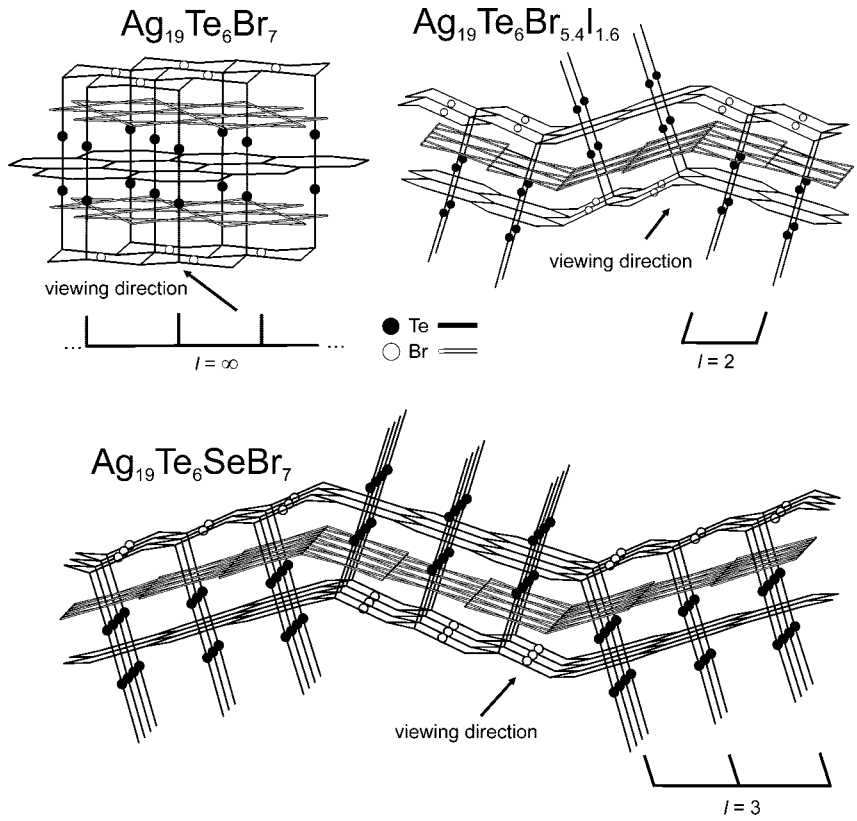

Figure 5. Structure sections of the anion substructures of $Ag_{19}Te_6Br_7$, $Ag_{19}Te_6Br_{5.4}I_{1.6}$, and $Ag_{19}Te_5SeBr_6$. The structure parameter l (for details, see text) is defined by the number of neighboring Q_4 unit rods derived after a projection into the viewing directions stated. This parameter is suitable to demonstrate the structure relation between the three different representations. The value of l is connected with a different grade of shear/shift-effects starting from a strong effect for $l = 2$ up to no shear/shift in case of $l = \infty$, resulting in a linear arrangement of the nets and strands.

continuation of the general structure principle. Selenide ions are distributed over all chalcogenide positions with a preference of the positions within the $(Te/Se)_4$ units (Te7/Se7) and (Te8/Se8) and only low selenide fractions on the positions within the planar area of (1) and at the contact position Te1 of (1) and (2) (see Table 6 and Figure 4).

Distances within the anion nets range from 4.48 to 4.65 Å for the 6^3 net (1), 4.43 to 4.60 Å for the $(Te/Se)_6$ rings (2), and 3.74 to 3.96 Å for the Br−Br distances within the Kagomé net (3). Bond distances are summarized in Supporting Information.

As shown in the previous cases a similar silver distribution around the chalcogenide nets and a silver gap in proximity of the halide nets are also present.

Despite the fact that no direct chemical bonding interaction is present between the different anion nets for all three compounds, the structural behavior points towards an indirect net interaction via the disordered silver substructure. The differentiated distribution of silver relative to the anion nets is obvious. Specifically, the more localized distribution of silver, represented by the smaller displacement parameters around the 6^3 nets (1) in comparison with the more diffuse and S-shaped distribution around (2), clearly substantiates this feature (see Figures 1, 3, and 4). These characteristics are present in all compounds under discussion. Also the silver tends to be more dislocated around the chalcogenide then around the halide substructure. It manifests in the existence of a gap in close proximity to the Kagomé net (3).

Homologies in the $Ag_{19}Q_6X_7$ Structure Family. The two quaternary compounds can be regarded as shear-shift variants of $Ag_{19}Te_6Br_7$. If we look parallel (1), along a selected direction and in such a way that (4) units which interpenetrate (1) are projected behind each other, one can define the number of neighbored rods as a structure parameter l (see Figure 5).

According to this parameter, the $Ag_{19}Te_6Br_7$ type is characterized by $l = \infty$. An endless number of Te_4 unit rods are present, independent of the applied viewing direction. The end caps of (4) also define (2) and therefore the orientation of all nets. Substitution within the anion substructure leads to a relative expansion or contraction of the structure fragments resulting in a certain distortion between the units. For instance the partial halide substitution of Br ($r_{ion}(Br^-) = 1.86$ Å, CN = 6 according to ref 45) by larger I ($r_{ion}(I^-) = 2.06$ Å, CN = 6) in $Ag_{19}Te_6Br_{5.4}I_{1.6}$ results in a relative expansion of the halide substructure. As a consequence a shear and shift of the structure units relative to each other occurred. Some halide subunits in (3), as denoted in Figure 3, bottom right section, are sheared relative to each other in combination with a relative expansion of the halide containing unit (2). If one defines the shear-line in (3) as the viewing direction the structure parameter becomes now $l = 2$.

Obviously the substitution of Te ($r_{ion}(Te^{2-}) = 2.07$ Å, CN = 6) by the smaller Se ($r_{ion}(Se^{2-}) = 1.84$ Å, CN = 6) in $Ag_{19}Te_5SeBr_7$ results in a drastic contraction of the chalcogenide substructure which has a more pronounced effect on (1) than on halide containing (2). Here, the structure

(45) Shannon, R. D. *Acta Crystallogr., Sect. A* **1976**, *32*, 751.

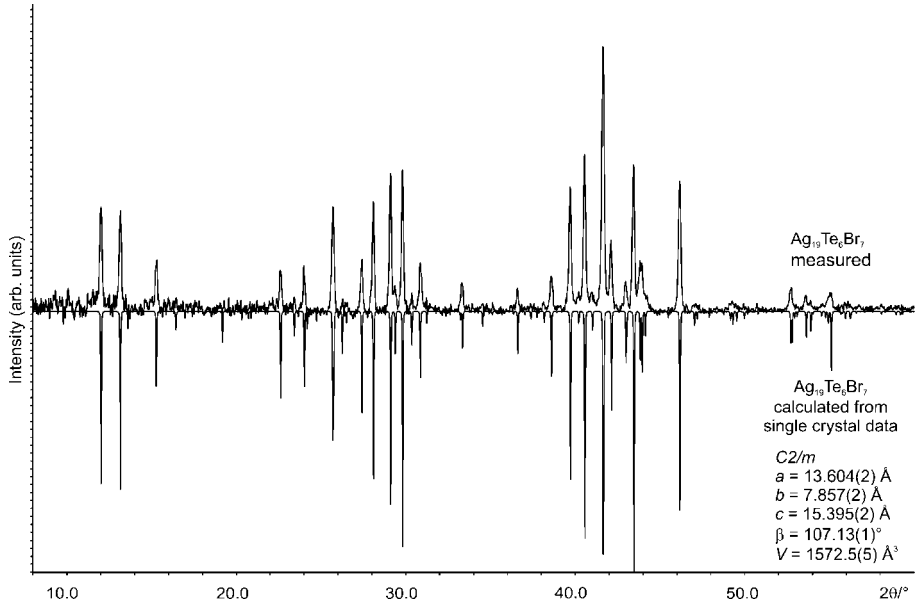

Figure 6. X-ray powder phase analysis of $Ag_{19}Te_6Br_7$ at 298 K. The *C*2/*m* model was used for the calculation.

parameter is $l = 3$. From a structure chemical point of view the question arises at this point if a structure parameter $l = 1$ or $l > 3$ exists in this system. This question will be addressed soon.

3.2. X-ray Powder Phase Analyses. The phase pure preparation of $Ag_{19}Te_6Br_7$ and $Ag_{19}Te_6Br_{5.4}I_{1.6}$ was substantiated from X-ray powder phase analyses (Figures 6–8). Calculated diffractograms derived from the single crystal structure determination data are in good agreement with the measured ones. In the case of $Ag_{19}Te_6Br_7$ the calculated diffractogram is based on the *C*2/*m* model. A calculated one in the $R\bar{3}m$ model shows no significant differences as discussed earlier on.

The phase analysis of $Ag_{19}Te_5SeBr_7$ showed the occurrence of a small AgBr impurity. Even after several homogenization and annealing steps the impurity did not vanish. Due to this fact we did not perform any additional determinations of physical properties, like for instance the electric conductivity. Such a determination can lead to the wrong results as shown in literature for pure $[Ag_4I]PO_4$[46] in contrast to the impure case[47]where the conductivity deviates by four orders of magnitude. Nevertheless, the measured powder diffractogram substantiates the correctness of the structure determination.

3.3. Impedance Spectroscopic Investigations. The total conductivity of $Ag_{19}Te_6Br_7$ and $Ag_{19}Te_6Br_{5.4}I_{1.6}$ was determined by impedance spectroscopy using ion blocking gold electrodes. Both compounds show an Arrhenius type behavior with conductivities in the range of related silver(I) chalcogenide halides and polychalcogenide halides (see Table 7).

Compared with Ag_5Te_2Cl the total conductivity is enhanced by one order of magnitude at room temperature for both compounds and is comparable to the values of $Ag_{10}Te_4Br_3$. In contrast to the latter, $Ag_{19}Te_6Br_7$ shows no phase transitions (see Section 3.4) and conductivity changes (see Figures 9 and 10) near room temperature which is favorable for room temperature applications. The conductivity of $Ag_{19}Te_6Br_{5.4}I_{1.6}$ at room temperature is as high as that of β-Ag_3SBr and exceeds AgBr by three orders of magnitude.

The partial substitution of bromide by iodide has no significant influence on the total conductivity. In contrast, a reduction of the activation energies can be observed from the ternary to the quaternary compound. For α-$Ag_{19}Te_6Br_7$ the activation energy reaches 0.19 eV while an increase to 0.32 eV is found for β-$Ag_{19}Te_6Br_7$. As stated in the introduction section Beeken et al. reported on the electric properties of Ag_3TeBr, and they found an activation energy of 0.35 eV between 150 and 400 K.[26] This value is very

Table 7. Selected Total Conductivities of Silver(I) Chalcogenide Halides and Silver(I) Polychalcogenide Halides

compound	σ (Ω^{-1} cm^{-1})	T (K)	reference
$Ag_{19}Te_6Br_{5.4}I_{1.6}$	1.1×10^{-2}	323	this work
	4.9×10^{-3}	298	this work
	2.0×10^{-3}	273	this work
	4.7×10^{-4}	243	this work
	2.3×10^{-5}	203	this work
α-$Ag_{19}Te_6Br_7$	9.3×10^{-4}	263	this work
	3.5×10^{-4}	243	this work
β-$Ag_{19}Te_6Br_7$	2.1×10^{-5}	203	this work
β-$Ag_{10}Te_4Br_3$	5.4×10^{-2}	323	7
γ-$Ag_{10}Te_4Br_3$	1.9×10^{-2}	303	7
δ-$Ag_{10}Te_4Br_3$	4.1×10^{-3}	273	7
	6.9×10^{-4}	243	7
	2.7×10^{-5}	203	7
β-Ag_5Te_2Cl	1.4×10^{-3}	323	24
	1.3×10^{-4}	298	24
β-Ag_3SBr	$\sim 5 \times 10^{-3}$	298	48
AgBr	1×10^{-6}	298	49

(46) Oleneva, O. S.; Kirsanova, M. A.; Shestimerova, T. A.; Abramchuk, N. S.; Davliatshin, D. I.; Bykov, M. A.; Dikarev, E. V.; Shevelkov, A. V. *J. Solid State Chem.* **2008**, *181*, 37.
(47) Takahashi, T.; Ikeda, S.; Yamamoto, O. *J. Electrochem. Soc.* **1972**, *18*, 477.
(48) Kawamura, J.; Shimoji, M. *Solid State Ionics* **1981**, *3/4*, 41.
(49) Maier, J. *Mater. Res. Bull.* **1985**, *20*, 383.

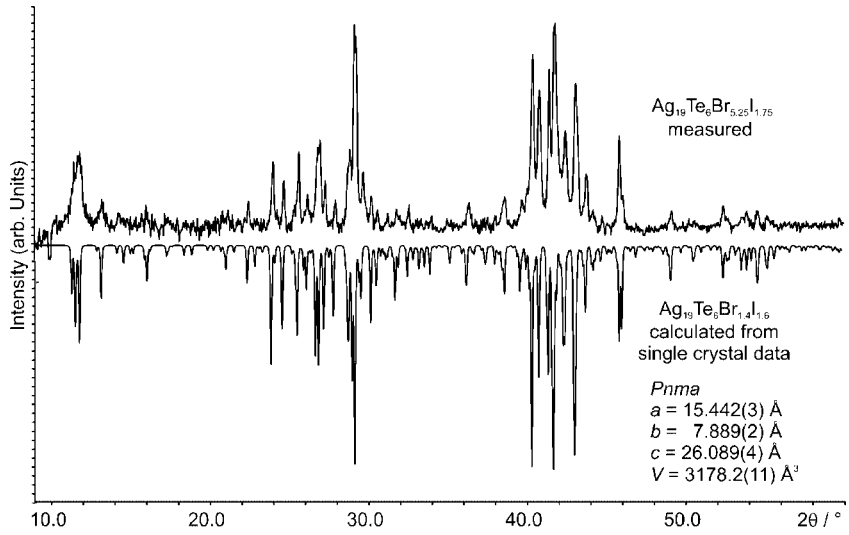

Figure 7. X-ray powder phase analysis of $Ag_{19}Te_6Br_{5.4}I_{1.6}$ at 298 K.

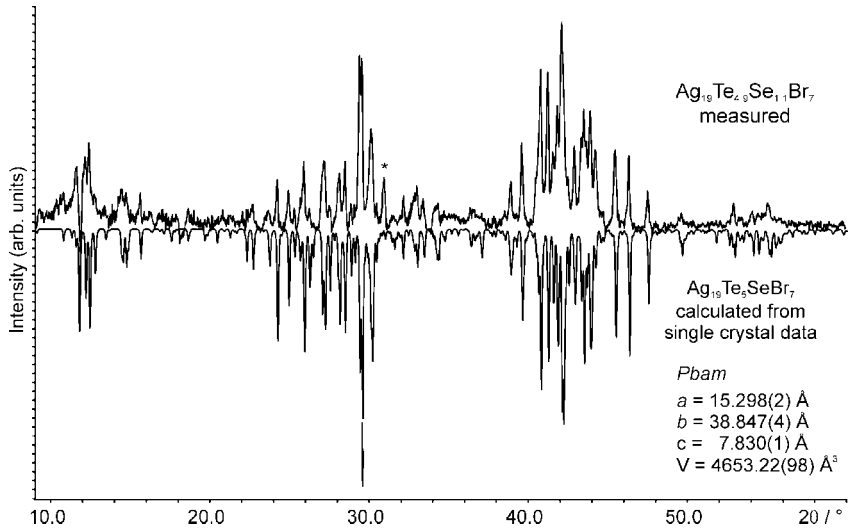

Figure 8. X-ray powder phase analysis of $Ag_{19}Te_5SeBr_6$ at 298 K. * represents a AgBr reflection.

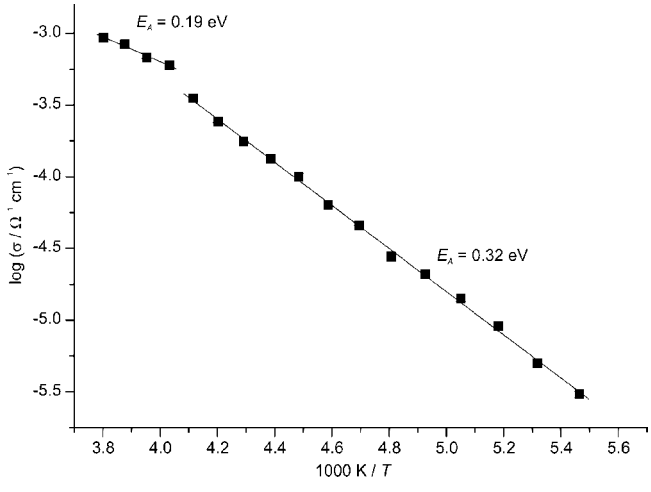

Figure 9. Arrhenius representation of the total conductivity of $Ag_{19}Te_6Br_7$ measured in the temperature range of 183−273 K. Activation energies are derived from the slopes of the linear sections.

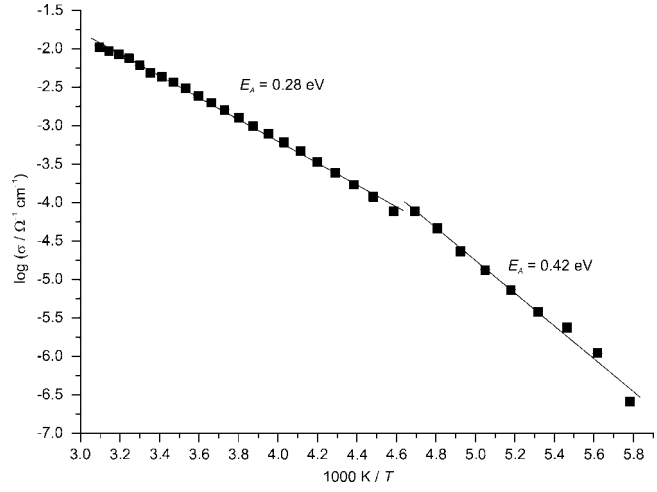

Figure 10. Arrhenius representation of the total conductivity of $Ag_{19}Te_6Br_{5.4}I_{1.6}$ measured in the temperature range of 173−323 K. Activation energies are derived from the slope of the linear sections.

close to the determined activation energy for β-$Ag_{19}Te_6Br_7$. Activation energies of 0.28 and 0.42 eV were achieved after the partial halide substitution for $Ag_{19}Te_6Br_{5.4}I_{1.6}$.

3.4. Thermal Analyses. DSC measurements were performed for all silver(I) chalcogenide halides in the temperature range of 113 to 873 K. All compounds decompose

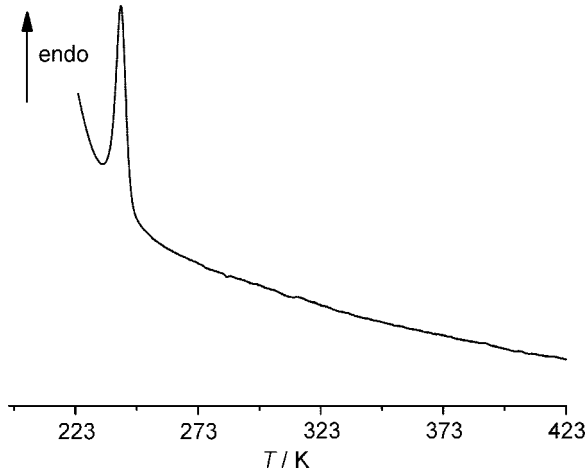

Figure 11. DSC measurement for $Ag_{19}Te_6Br_7$ in the temperature range of 223−423 K. An endothermic effect was found at 235 K representing the ordering temperature of silver.

peritectically, characterized by broad thermal effects at temperatures slightly above 673 K. $Ag_{19}Te_6Br_7$ decomposes at 719 K to Ag_2Te, AgBr, and $Ag_{23}Te_{12}Br$. The two quaternary compounds have reduced decomposition temperatures to the respective silver halides and silver chalcogenides of approximately 693 ($Ag_{19}Te_6Br_{5.4}I_{1.6}$) and 708 K ($Ag_{19}Te_5SeBr$). An endothermic effect was detected in the low temperature region of $Ag_{19}Te_6Br_7$ at 235 K (Figure 11).

This thermal effect is in good accordance with the small conductivity jump at 243 K visible in the impedance experiment. A single crystal structure determination was performed at temperatures below this thermal effect in order to evaluate the structural changes during this phase transition. Preliminary results of the structure refinement point towards a silver ordering in combination with a severe crystallographic twinning problem. The structure refinement is still in progress and results will be reported soon.

No thermal effects were found for the quaternary compounds in the low temperature region. Obviously the silver ordering temperature is drastically reduced for the quaternary compounds. This reduction was also observed for comparable systems like Ag_5Q_2X [21,24] or $Ag_{10}Q_4X_3$.[8,9] The change of the slope of the conductivity in the case of $Ag_{19}Te_6Br_{5.4}I_{1.6}$ cannot be correlated to a thermal effect in DSC experiments.

4. Conclusion

Three new silver(I) chalcogenide halides were prepared by solid state reactions from the elements and silver halides. A peritectic decomposition behavior was observed by thermal analyses with binary chalcogenides and halides and $Ag_{23}Te_{12}X$ as decomposition products. All compounds are stable in air and are not light sensitive over months. A huge silver mobility results in high disorder within the cation substructure and is the origin of polymorphism. The total conductivities and the low activation energies of $Ag_{19}Te_6Br_7$ and $Ag_{19}Te_6Br_{5.4}I_{1.6}$ point towards an enhanced charge carrier mobility capable of being used in electrochemical applications around room temperature.

All efforts to prepare Ag_3TeBr with solid state melting reactions, mineralization routes using tellurium halides, or hydrothermal syntheses failed completely. The only product we achieved in our group was $Ag_{19}Te_6Br_7$.

Acknowledgment. The authors thank the Deutsche Forschungsgemeinschaft DFG (SFB 458, Project A5) for the kind support of this project and Dr. Hinrich-Wilhelm Meyer for the help with the impedance experiments. All DSC experiments were done by Mrs. Wilma Pröbsting which is gratefully acknowledged.

Supporting Information Available: Additional crystallographic data of the three title compounds (PDF) and CIF files. This material is available free of charge via the Internet at http://pubs.acs.org.

CM800425U